

Dynamic transition of nanosilicon from indirect to direct-like nature by strain-induced structural relaxation

Cite as: AIP Advances **11**, 095319 (2021); <https://doi.org/10.1063/5.0050581>

Submitted: 16 March 2021 • Accepted: 31 August 2021 • Published Online: 29 September 2021

Kevin Mantey,  Huw Morgan,  Jack Boparai, et al.



View Online



Export Citation



CrossMark

ARTICLES YOU MAY BE INTERESTED IN

[Enhancing mechanical properties of NbZrMo alloy by maximizing configurational entropy from first-principles calculations](#)

AIP Advances **11**, 105001 (2021); <https://doi.org/10.1063/5.0057624>

[Growth of highly conductive Al-rich AlGa_N:Si with low group-III vacancy concentration](#)

AIP Advances **11**, 095119 (2021); <https://doi.org/10.1063/5.0066652>

[Earth factories: Creation of the elements from nuclear transmutation in Earth's lower mantle](#)

AIP Advances **11**, 105113 (2021); <https://doi.org/10.1063/5.0061584>

Call For Papers!

AIP Advances

SPECIAL TOPIC: Advances in
Low Dimensional and 2D Materials

Dynamic transition of nanosilicon from indirect to direct-like nature by strain-induced structural relaxation

Cite as: AIP Advances 11, 095319 (2021); doi: 10.1063/5.0050581

Submitted: 16 March 2021 • Accepted: 31 August 2021 •

Published Online: 29 September 2021




View Online



Export Citation



CrossMark

Kevin Mantey,¹ Huw Morgan,²  Jack Boparai,¹  Zain Yamani,³  Ersin Bahceci,⁴ 
and Munir Hasan Nayfeh^{1,a)} 

AFFILIATIONS

¹Department of Physics, University of Illinois at Urbana-Champaign, 1110 W. Green Street, Urbana, Illinois 61801, USA

²Department of Physics, Aberystwyth University, Penglais, Aberystwyth, Ceredigion SY23 3BZ, United Kingdom

³Department of Physics, King Fahd University, Dhahran 34463, Saudi Arabia

⁴Department of Metallurgical and Materials Engineering, Iskenderun Technical University, 31200 Hatay, Turkey

^{a)} Author to whom correspondence should be addressed: m-nayfeh@illinois.edu

ABSTRACT

Silicon nanoclusters exhibit light emission with direct-like ns– μ s time dynamics; however, they show variable synthesis and structure, optical, and electronic characteristics. The widely adopted model is a core–shell in which the core is an indirect tetrahedral absorbing Si phase, while the shell is a network of re-structured direct-like H–Si–Si–H molecular emitting phases, with the two connected via back Si–Si tetrahedral bonds, exhibiting a potential barrier, which significantly hinders emission. We carried out first-principles atomistic computations of a 1-nm Si nanoparticle to discern the variabilities. Enlarging the network reduces the potential barrier monotonically to a finite limit not sufficient for strong emission to proceed while inducing a path to quenching of emission via a conical crossing between the excited and ground states. However, enlarging the network is found to induce strain and structural instability, which causes structural relaxation that creates a direct path for emission without crossing the barrier. Following emission, the particle relaxes back to the indirect ground structure, which completes the cycle. The results also confirm the pivotal role of HF/H₂O₂ etching in synthesizing the core–shells and affording control over the molecular network. Measurements using synchrotron and laboratory UV excitation of thin films of 1-nm Si particles show good agreement with the simulation results. It is plausible that the relaxation is behind the stimulated emission, gain, or microscopic laser action, reported earlier in macroscopic distributions of 1- and 3-nm Si nanoparticles.

© 2021 Author(s). All article content, except where otherwise noted, is licensed under a Creative Commons Attribution (CC BY) license (<http://creativecommons.org/licenses/by/4.0/>). <https://doi.org/10.1063/5.0050581>

I. INTRODUCTION

Since the first observation of strong luminescence in free-standing, laboratory prepared ultrasmall silicon crystals/nanoparticles,^{1–4} concerted experimental,^{5–7} theoretical, simulation, and computation efforts^{8–16} have been initiated to discern why and how the luminescence commences and to present structural prototypes that may explain the keys to synthesis and the optical, electronic, and mechanical characteristics of the material. The focus was on a 1-nm diameter nanoparticle since it is amenable to both experimentation and atomistic simulation and computation,

which allow direct comparison between theory and experiment. The characteristics include strong, near direct-like, wide-band visible luminescence peaked at 2.75 eV (440 nm), nanosecond time dynamics, absorption in the UV range at \sim 3.2 to 3.5 eV with a Stokes shift of 0.5–0.6 eV, strong specific UV and visible emission bands, H-termination and passivation, high Coulomb blockade, Si-to-metal phase transition at high pressure, and photo- and structural stability. In parallel, the material was put to use by incorporation in advanced applications, affording a variety of interesting high-tech device prototypes,^{5–7} such as UV photo-detectors,^{17,18} nonlinear optics,^{19,20} solid state converters for white lighting²¹ charge-based

nanomemory,²² super electrical storage (capacitor),²³ solar cells,²⁴ electrochemical glucose sensors,²⁵ biofuel cells,²⁶ and high-pressure sensors.²⁷

Local density approximation (LDA) simulations and tight binding (TB) theory^{8,9} were used to construct a prototype of the hydrogen-terminated 1-nm particle. Starting out with the tetrahedral structure (TD) $\text{Si}_{29}\text{H}_{36}$, a fluorescing molecule based on an intrinsic defect is created by stripping two hydrogen atoms from two nearby silicon atoms and allowing the “bare” Si atoms to move closer to form a Si–Si bond, which results in the prototype $\text{Si}_{29}\text{H}_{34}$. Computations of the structure confirm that this prototype does produce wide-band luminescence with a lifetime in the nanosecond regime. Moreover, the computations show that the excited particle is described by a double-well system, coupled by a potential barrier, one of which is a TD absorption well and the other is a molecular emission well. Despite this success, the model has shortcomings. The potential barrier between the wells is a large prohibitive 0.5 eV barrier, which essentially blocks emission, especially at room temperature. Moreover, contrary to measurements, which show that the luminescence appears at a photon excitation of ~ 3.2 to 3.5 eV, with a Stokes shift of 0.6 eV, the luminescence in the model appears only with high-photon energy absorption/excitation at ~ 4.9 eV and emission with a large (~ 2 eV) Stokes shift.

It would be interesting to analyze prototypes that have networks of multiple molecular sites to probe if multiplicity of sites would alleviate the problem. However, it is not clear how such multiplicity would affect the height of the potential barrier and the TD symmetry and elasticity or strain in the particle.²⁷ For instance, the original structure $\text{Si}_{29}\text{H}_{36}$ has a TD symmetry, while the $\text{Si}_{29}\text{H}_{34}$ structure breaks the TD symmetry. Moreover, it is not clear how other site configurations would affect the structural distortion and relaxation, especially under UV excitation to high-lying excited states. In addition, it would be interesting to discern how the interdependency among those factors would affect the molecular and electronic structures, hence optical selection rules and absorption and emission processes, and emergence of direct-like fast emission nature.

In this paper, we examine the transition of the indirect dull nature of bulk silicon to direct-like nanosecond emission (up to several nanoseconds)²⁸ in nanosilicon at the limit of size (sub-3-nm). We use laboratory and synchrotron UV excitation as well as comprehensive advanced atomistic simulation and computations to calculate the energy surfaces of the ground state and excited states in a 1-nm silicon particle for a variety of networks of coupled surface Si–Si molecular emission sites. We also calculate the structures under UV-induced structural relaxations in the excited states that include induced structural surface reconstruction and bulk nuclear relaxation in the ground and excited states as well as various structural symmetries. Recent advances in computation protocols have provided the capability of providing excited state energy gradients with respect to the nuclear positions, which allowed refinements via excited state geometry relaxation.²⁹ Moreover, while calculated absolute energies may become more accurate, it would be interesting to examine differences in energy between similar configurations and hence basic trends even for more reliability and usefulness for experimental predictions. In our computations, we obtain the wave functions, the height of the barrier, and the depth of the wells and evaluate their structural stability as well as the time dynamics of

emission across the wells and the barrier. The results show that increasing the size of the network causes the transition potential barrier to a monotonic drop to the 0.06 eV barrier and the molecular well to collapse on one side, turning into a half-open well, which leads to an excited state-ground state conical crossing that quenches emission. Moreover, the multiplicity of molecular sites increases the structural strain and instability, causing the excited particle to structurally relax to lower states with a variety of symmetries, which causes the absorbed energy to be transferred into the top of the transition barrier region of those lower states, followed by strong fast emission without traversing the barrier. The strong excited state relaxation lowers the absorption to 3.29 eV and reduces the Stokes shift to 0.6 eV in agreement with laboratory measurements taken on 1-nm particles in the range of 3.2–3.5 eV using low photon energy as well as using excitation with synchrotron UV radiation taken in the range of 4.8–7.5 eV. Understanding the process would not be only of scientific interest but it enables a better design of the material into advanced high-tech functionality and device applications. Moreover, a direct-like nanof orm of silicon with strong fluorescence activity would be highly useful for integration of electronics and optics.

II. THEORETICAL SETUP AND METHODOLOGIES

A. 1-nm silicon nanoparticle system

The concept of direct nature in nanosilicon, which affords a luminescent character, is based on re-arranging the silicon atoms in a bulk-like particle, especially those on the surface such that they form additional bonds. Figure 1(a) shows a TEM image of an example of nanosilicon, namely, 1-nm Si particle, which has been prepared in the laboratory. Figure 1(b) shows a computer prototype of the bulk-like configuration of this particle produced by cutting out a 1-nm sphere from a $\langle 100 \rangle$ single crystal silicon wafer. This cutout contains 29 silicon atoms with 36 broken bonds. We terminate the broken bonds in the particle with hydrogen to “freeze” the particle in the bulk structure, forming $\text{Si}_{29}\text{H}_{36}$. A direct nature of this $\text{Si}_{29}\text{H}_{36}$ nanoparticle, which affords it a luminescent character, can be explained with the aid of Fig. 1(c). It is based on reducing the number of H atoms and re-arranging the bonding of the “stripped” surface Si atoms. Consider a pair of second nearest surface silicon atoms (separated by 5.4 Å), each of which, terminated by two H atoms, is stripped of a hydrogen atom, which can then move endothermic closer to each other such that they form a new H–Si–Si–H bond of length 2.36 Å, the tetrahedral bond length. Experimentally, hydrogen atoms are stripped by the oxidizer H_2O_2 present in the synthesis solution, which causes a reaction such that an H_2O_2 molecule may strip two H atoms from adjacent Si sites forming two water molecules. Due to the significant reduction of elasticity in ultrasmall particles, the “stripped” atoms can appreciably move simultaneously closer to reconstruct.^{11,15,30} Effectively, the process results in two water molecules and a $\text{Si}_{29}\text{H}_{34}$ particle in which a H–Si–Si–H dimer-like molecule forms while being coupled to the rest of the particle by attachment to the underlying silicon atoms (bulk tetrahedral phase) through back tetrahedral silicon bonds. This is similar to a $\langle 100 \rangle$ Si surface reconstruction dimer. However, the reconstructed surface bonds here do not have double bonds like in the $\langle 100 \rangle$ dimer case because here each of the atoms has a single hydrogen termination as well. Thus, such reconstructed

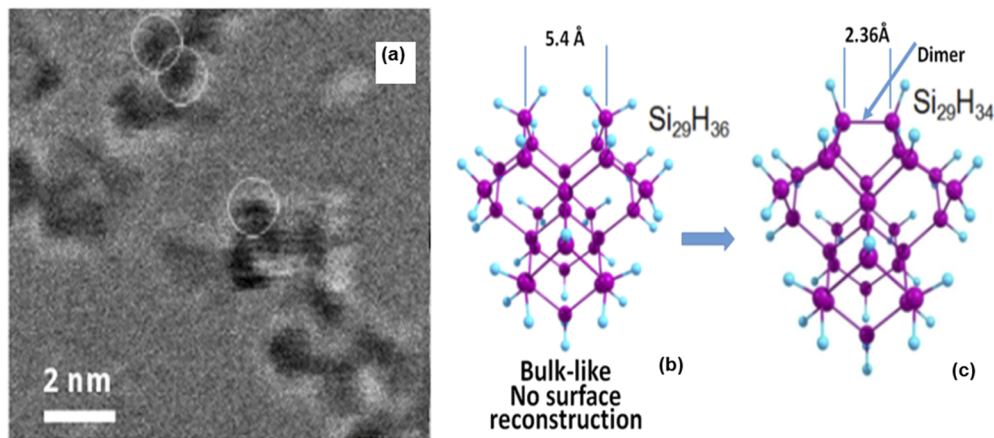


FIG. 1. (a) Transmission electron microscopy (TEM) image of the 1-nm silicon nanoparticle deposited on a graphite grid. (b) Computer model of 1-nm silicon particles ($\text{Si}_{29}\text{H}_{36}$) in the “bulk configuration.” It shows next nearest silicon atoms separated by 5.4 Å (the characteristic lattice spacing) and they are not bonded to each other. Each of those atoms is bonded to two hydrogen atoms (di-hydride terminated). (c) Surface reconstruction dimer model. For a pair of di-hydride terminated silicon atoms in the $\text{Si}_{29}\text{H}_{36}$ “bulk configuration,” two hydrogen are removed and the silicon atoms move closer to 2.36 Å and are bonded. This bond is referred to as a dimer. The small atoms on the surface with one bond are hydrogen (light blue). The largest atoms, with four bonds, represent silicon (purple).

bonds are referred to as dimer-like. Those dimer-like sites afford the particle a molecule-like nature, and in some sense, this ultrasmall particle constitutes the transition between the solid and molecule or “super molecule.” In fact, the $\text{Si}_{29}\text{H}_{24}$ particle lies at the edge of the silicon-like sp^3 bonding and the carbon-like sp^2 bonding. As more hydrogen is stripped to numbers below 24, sp^2 bonding forms while the bandgap sharply drops. Eventually, the bandgap collapses and the particle becomes conducting.³⁰

B. Previous computations of 1-nm Si nanoparticle

Because of its unique structure of being not purely solid nor molecule, and the emergence of novel characteristics and applications, the 1-nm nanoparticle has attracted extensive attention, both experimentally and theoretically. The small size lends itself well to the application of atomistic first-principles quantum mechanical computational methods. The structure and electronic properties of the silicon cluster have been studied by numerous methods, including tight binding,^{9,31} empirical pseudo-potentials,³² GW–Bethe Salpeter (GW–BSE),^{33,34} density functional theory (DFT),^{35–37} and quantum Monte Carlo (QMC).^{38,39} However, it has been noted that while significant progress has been made in matching computational models with experimental data for clusters larger than 2 nm, there remains a difficulty in interpreting properties in the smaller regime, where the surface atoms become a significant portion of the volume.⁴⁰ Indeed, previous work has noted that experimentally determined energy levels of particles larger than 2 nm can be fit well even with a simplified quasi-particle in a box confinement model, while smaller silicon nanocrystals do not.⁴¹ This indicates that below 2 nm, the molecular nature of the particles becomes increasingly important. Therefore, when discussing the smallest of the preferred sizes, the 1-nm silicon particle, an understanding of the surface structure and composition is crucial.

A good starting point for investigating the structure of the 1-nm silicon particle is taking a spherical cutout of bulk and replacing any

dangling bonds with hydrogen. The resulting structure, $\text{Si}_{29}\text{H}_{36}$, will be referred to as the bulk-like configuration. The particle has a tetrahedral core of five silicon atoms, surrounded by 24 silicon atoms on the surface of which 12 have single H-termination and the other 12 have di-hydride H-termination. It was argued earlier that there is a strong indication that the preferred sizes come from the preference for mono-hydride termination. In the bulk-like configuration, the 1-nm particle has just as many mono-hydride and di-hydride surface terminations. This may therefore not appear to be very stable in light of the mono-hydride preference. Compare this, however, to the structure created by adding just one more layer of silicon atoms to the bulk configuration, which would have 12 di-hydride and 24 tri-hydride terminations.

While there is no spherical cutout of the bulk that will leave only mono-hydride surface atoms, it is possible via surface reconstruction of the bulk configuration to obtain a 1-nm silicon particle with only mono-hydride termination. The 12 di-hydride silicon atoms in the bulk configuration sit such that they form six pairs. If two hydrogen atoms are removed from each silicon pair and a bond between them is added, the surface now only has mono-hydride termination. This is similar to a (100) Si surface reconstruction dimer, so such reconstructed bonds are referred to in the literature as a dimer (to avoid confusion, note that the reconstructed surface bonds here do not have a double bond nature like in the (100) dimer case because here the atoms each have a single hydrogen termination as well).

To compare possible structures for the 1-nm silicon particle, previous calculations have primarily made predictions and comparisons with the experimental absorbance measurements. In particular, the absorption edge at the “bandgap” energy has been particularly focused on. This bandgap was experimentally determined to be 3.5 eV.³⁹

For the bulk-like configuration $\text{Si}_{29}\text{H}_{36}$ with no surface reconstruction, Delerue *et al.*⁴² calculated a gap of ~5 eV using a tight binding (TB) method. Using fixed-node diffusion quantum Monte

Carlo (QMC) methods, Mitas *et al.*³⁹ and Williamson *et al.*^{43–45} also found that the bulk-like configuration had a bandgap larger than the experimental value. Mitas *et al.* calculated a gap of 4.8 eV, while Williamson *et al.* reported 5.3 ± 0.1 eV. Time dependent density functional theory (TDDFT) has also been employed by Vasiliev and Martin to predict an absorption edge of 4.2 eV.⁴⁶

These initial calculations found the bandgap of the bulk-like configuration to be significantly greater than the experimental value, so various changes in the structure were proposed. It was found that either double bonded Si=O surface oxidation or bridging Si–O–Si oxidation will reduce the bandgap according to tight binding^{47–49} and TDDFT^{50,51} calculations. In addition, surface reconstruction via the formation of one or more dimers will also reduce the bandgap according to TB,^{2,47} QMC,³⁹ and TDDFT.^{46,52} However, there is disagreement in the literature over which structure fits best with the experimental evidence. After comparing structures, Rao *et al.*⁵³ and Mitas *et al.*^{39,40} concluded that the fully reconstructed Si₂₉H₂₄ with six dimers fits the data best. However, more recent reports in 2005 by Lehtonen and Sundholm⁵⁴ and in 2008 by Zhanpeisov and Fukurnura⁵⁵ provided calculations and interpret structures with only bulk-like configuration and hydrogen termination to be best fits to the data. Also in 2009, Garoufalidis and Zdetsis considered the purely hydrogenated bulk configuration structures to be ruled out although note that surface oxygen in addition to dimers may play a role.⁵²

To resolve these debates over surface reconstruction, it would be advantageous to turn away from bandgap or absorption predictions and measurements and use instead a technique that could give a more direct fingerprint of the surface state itself. If the particles are quite homogeneous in not just size but also molecular structures, it is possible to use Raman spectroscopy of the particles in solution to provide information on vibrational modes of the particles. Such an experiment was successfully carried out by Rao,⁵⁶ providing measurements of the frequency of Raman active modes and the polarization of light scattering by these modes. The Raman measurements, when compared to the calculated vibrational modes, indicate Si₂₉H₂₄ as the most likely structure for the 1-nm silicon particle. This matches what is expected from the fabrication procedure. The results from the bulk-like configuration Si₂₉H₃₆ were the worst fit to the measured peaks, giving independent validation that Si₂₉H₂₄ is the more likely structure compared to Si₂₉H₃₆ based on comparison of measured absorption to calculated spectra.

C. Present functional/basis and simulation strategy

In DFT theory and calculations, different types of functional and basis sets can be used and most computing software programs are plane wave or Gaussian based on pros and cons. There is not a single choice that can do everything, however. The choice among them depends on the phenomena to be studied and the system to be calculated. For instance, some functionals are able to reasonably predict structures but sometimes underestimate the bandgap and other functionals that describe that the bandgap well can often overestimate the lattice parameter. There are several comparative studies devoted to comparing the accuracy of the functional for predicting the structural and electronic properties of molecules and solids.^{57–61} The main conclusion is that none of the available functionals are able to describe all electronic, optical, structural, mechanical, and vibrational properties of the studied systems at the same time, and

their results are strongly dependent on the basis set or the potential used. For the system at hand, the 1-nm silicon particle is not a pure solid or a pure molecule. In our group, we have found that the B3LYP functional is a reasonable compromise for carrying out both the solid state and the molecular characteristics simultaneously with reasonable accuracy for comparison with experiment. We have determined structural, electronic, energy, optical, mechanical, and vibrational properties. The choice of this functional and/or basis set was based on the ability to reproduce the experimental data, with emphasis on the lattice parameter and bandgap energy, as the accurate calculation of the bandgap is a fundamental step in simulations applied to solid-state systems.

Our strategy is to use advances in atomistic simulations in terms of the hybrid functional to provide improved calculations. We obtain the equilibrium ground state geometries for all structures using DFT with the B3LYP hybrid functional using the quantum computational package GAMESS (General Atomic and Molecular Electronic Structure System)^{29,30} using the 6-311G(d,p) basis set. We also used the same functional with the TURBOMOLE quantum computational package with TZVP basis, which is a triple split valence basis with polarization functions added for each atom.²⁹ It should be noted that the PBE0 hybrid functional can also be used in this application. In general, for bulk or large nanostructures, the B3LYP functional might yield unsatisfactory^{62,63} atomization energies (~12% error for Si). The lattice constants (~1% error for Si) and bulk moduli (9% error for Si) are not particularly well-predicted by this functional as well. The ultrasmall Si nanostructure considered here, however, is expected to behave as a super molecule, Si₂₉H_x molecule, which may make it amenable to the B3LYP functional with better accuracy than larger silicon or other semiconductor structures. Moreover, B3LYP already provides structural optimization comparable to the simple PBE functional. Previous calculations showed that the B3LYP functional provides results on energy gaps of zinc-blende and wurtzite structured III–V materials that are close to experimental values than with PBE0. Agreement with experimentally derived bandgaps at characteristic points in the first Brillouin zone (BZ) is at least as good as that obtained with correlated calculations, perturbation theories, and screened exchange functionals. Both PBE and B3LYP provide reasonable bond lengths and angles within 0.02 Å and 2°, respectively. PBE (and any GGA) is known to underestimate HOMO–LUMO gaps, unlike hybrid functionals, such as B3LYP. Therefore, B3LYP is better suited for optical property calculations. The downside is that the hybrid functional tends to be several orders of magnitude more expensive than GGA in the plane wave basis set [Vienna *Ab initio* Simulation Package (VASP)].

The density functional B3-LYP is the Becke-3-Parameter hybrid functional. The exchange part consists of $0.8^* \text{LDA} + 0.72^* \text{B88} + 0.2^* \text{HF}$. The correlation used is $0.19^* \text{LDA(VWN)} + 0.81^* \text{LYP}$. We will use it for the calculation of the molecular/electronic structure including the double well of the dimer-like structure used with optimization in the ground state. Relaxation of the nuclear coordinates to minimize the energy in the ground state gives paths on the on-state potential energy surfaces of both the ground and excited states. Those are more relevant to absorption. We obtain the equilibrium ground/excited state geometries for several structural variations, which will give us a means to obtain trends.

These functions are discretized on numerical grids. Adding high frequency (small wavelength) plane waves increases the energy cutoff and will therefore require increasingly finer grid points to be described. This will, however, quickly increase computational cost. Since a sensible cut-off energy is not known *a priori*, the calculation was begun by convergence testing. Basic calculations were repeated for our system, increasing the cut-off energy and checking for property convergence. The presented results were calculated using spherical integration using the Lebedev's spherical grid, with a spherical grid size of 4, i.e., the grid point is 434. The radial integration used is the Chebyshev second kind (scaling 3). In this, the radial grid size is 6, while the integration cell size is 15. The partition function used is the Becke partition function, with the partition sharpness being 3. It is to be noted that in the integration for the density functional, the angular coordinate is the 302 Lebedev spherical shell of grid points, while the radial coordinate consists of 63 points, giving an overall of ~20 k grid points.

The second theory level uses the B3LYP functional in the TURBOMOLE with optimization in the excited state as well as in the ground state. The calculation of the excited state potential energy surface of $\text{Si}_{29}\text{H}_{24}$ was done at the TD-DFT level using the B3LYP functional with the TURBOMOLE quantum computational package.⁶⁴ The TZVP basis was used, which is a triple split valence basis with polarization functions added for each atom.^{65–67} The excited state energy gradients with respect to the nuclear positions are available, allowing excited state geometry relaxation.^{68,69} It is to be noted that the excited state optimization has become available only in recent advances in computation protocols. It affords the capability of obtaining excited state energy gradients with respect to the nuclear positions, which allowed refinements via excited state geometry relaxation. It is to be noted that the second derivative of the energy with respect to the nuclear positions (Hessian) can be calculated analytically for small molecules, but for larger molecules, a numeric differentiation is necessary. This is done by calculating the energy in the equilibrium position and then, for each atom, performing a gradient calculation at a structure with that atom displaced slightly along each Cartesian.

While calculated absolute energies may become more accurate, differences in energy between similar configurations give basic trends and reliability and usefulness for experimental predictions. In fact, molecular properties in multi-electron systems are best phrased in terms of differences between structures. Even minimal atomic basis sets can achieve predictions that on average only deviate from experiment, 0.05 Å for bond lengths and $\pm 10^\circ$ for bond angles.⁷⁰ Predictions of molecular properties by a triple valence basis introduced in the TZVP allow improvements, bringing bond lengths within 0.02 Å and bond angles to 3° on average. The molecular/electronic structure optimized in the ground state is relevant to absorption, and relaxation of the nuclear coordinates in the excited state is more relevant to emission and contributes to the Stokes shift. This also allows answering the question of the existence and stability of the outer well minimum, which could not be determined with relaxation in the ground state. Additionally, knowledge of how much the barrier between the two wells can be reduced by relaxation in the excited state determines if direct excitation over the barrier is energetically allowed.

The constraint in optimization of the dimer used was not the NEB (Nudged Elastic Band), rather it was static snaps. In the

process, one dimer in the structure is stretched/infated to a set value while allowing the rest of the nuclear coordinates to relax. This was repeated at multiple dimer lengths, and the coordinates of the resulting structures were used as the reaction path to investigate a slice of the excited state energy surface. The constrained optimization process may be done while the system is in the ground state or in an excited state, which is used to construct a reaction path. For all structures considered in this paper, the coordinates maintained C_{2v} point group symmetry along this path.

The Brillouin zone (BZ) sampling used the k-points that are given relative to the basis vectors of the reciprocal unit cell according to Ref. 71 [$\sum (2n_i - N_i - 1/2N_i) \mathbf{b}_i$, where $i = 1, 2, 3$ and $n_i = 1, 2, 3$, and $N_i (N_1, N_2, N_3)$ and \mathbf{b}_i are reciprocal lattice vectors].

Finally, the paper was written in a way to highlight and bring out absolute as well as trends of the phenomenon. This was executed having in mind the inherent approximations usually employed in solving nonlinear many-body problems and the fast evolution of the computational procedures and packages and accuracies. This strategy is useful especially since the paper focuses on the nanostructure of the same size (1-nm) but with similar, small variations in the configuration (0 dimers, 1 dimer, 5 dimers, and 6 dimers) or degree of H-termination (36, 34, 26, and 24 H atoms). This procedure has provided additional comparison on differences.

III. THEORETICAL RESULTS—OPTIMIZATION IN THE GROUND STATE

A. Single molecular site

The equilibrium ground state geometries for all structures were obtained using DFT with the B3LYP hybrid functional using the quantum chemistry computational package GAMESS (General Atomic and Molecular Electronic Structure System)^{29,72–74} using the 6-311G(d,p) basis set. Given any position for the nuclei, even if not at the minimum of the ground state potential energy surface, time dependent density functional theory (TDDFT) can be used to obtain excited state energies and oscillator strengths. A series of calculations at different nuclear coordinates can therefore provide the excited state potential energy surface along a slice.

We start with the bulk-like configuration of 1-nm silicon nanoparticle $\text{Si}_{20}\text{H}_{36}$. Two adjacent hydrogen atoms are stripped and the silicon atoms at a spacing of 5.4 Å move closer to a spacing of 2.35 Å and form a dimer-like structure, H–Si–Si–H dimer-like site. We now compress or inflate the dimer-like bond and keep it in static equilibrium. We now use the time dependent density functional theory (TDDFT) to calculate the ground state and excited state energy surfaces using the B3LYP functional and the 6-311G(d,p) basis set in the quantum computational package GAMESS (General Atomic and Molecular Electronic Structure System). For a given dimer length, we optimized the geometry by allowing the other nuclear coordinates to relax to minimize the total energy. We then perform a series of similar calculations for a series of static inflations at different nuclear coordinates to construct the excited state potential energy surface along a slice. We investigated using this procedure the electronic/molecular structure of 1-nm silicon nanoparticle with a single H–Si–Si–H structure ($\text{Si}_{29}\text{H}_{34}$). Figure 2(a) shows the resulting energy level diagram of the particle, showing the energy of the ground state and the first excited state as well as the radiative

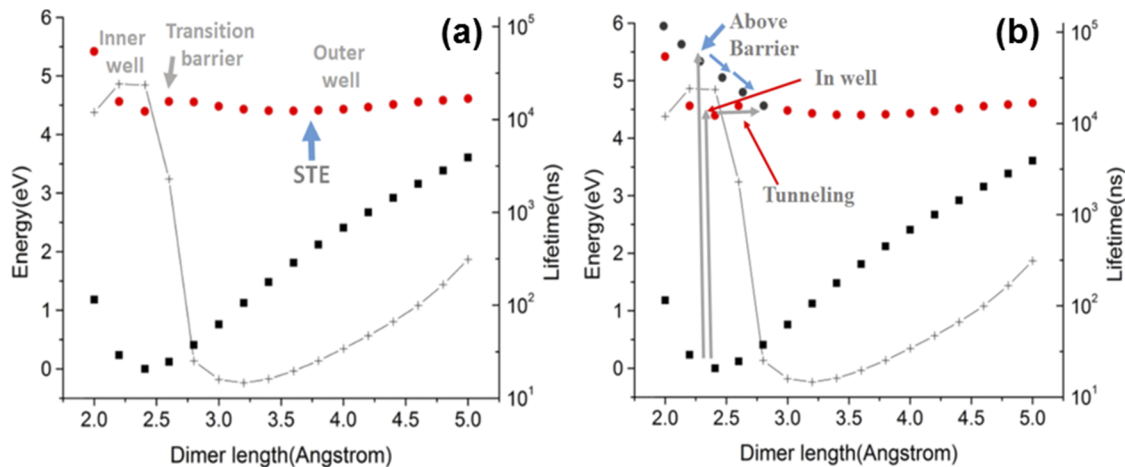


FIG. 2. Partial energy level diagram of the surface dimer showing the potential curves of the ground (■) and first excited (●) states (HOMO–LUMO) and radiative lifetime (+) of the 1-nm silicon nanoparticle with a single dimer reconstructed (configuration of $\text{Si}_{29}\text{H}_{34}$) as a function of dimer bond length d after it has been compressed or inflated from the equilibrium point at $d = 2.35$ Å. (a) labels the inner well and outer well [self-trapped exciton (STE)] and the transition barrier region. (b) labels excitation and emission pathways. It schematically shows two excitation pathways into the inner well. First minimum-to-minimum vertical excitation followed by quantum tunneling or thermal activation through the barrier; and second above-barrier excitation at higher photon energy followed by sliding (relaxation) into the outer well. The ground state and excited state energy surfaces are calculated using TDDFT with B3LYP functional and the 6-311G(d,p) basis set in the quantum computational package GAMESS (General Atomic and Molecular Electronic Structure System).

lifetime as a function of the bond length. A double-well structure connected by a potential barrier was found in the potential of the first excited state. The diagram labels the inner well (indirect-like well) and outer well (direct-like well) and the potential barrier in the transition region between the wells. The outer well is also labeled self-trapped exciton (STE). Note that it is only in the excited state that an outer well forms. One can, however, observe a kink in the ground state curve that lines up with the barrier in the excited state. The bandgap, which is defined as the minimum-to-minimum energy of the inner wells in the excited state and the ground state, is 4.4 eV. For comparison, a B3LYP-TDDFT calculation, which was done on the bulk configuration $\text{Si}_{29}\text{H}_{36}$ structure, with no dimers, yielded a bandgap of 4.5 eV. Therefore, at this level of theory, the bandgap is only reduced slightly by a single dimer. For illustration purposes, we represent the inner well with a parabola and the weakened bond outer well is also represented with a parabola. The bond length at which these two parabolas cross, i.e., the barrier area, will represent the point at which the two natures are strongly mixed and that the nature of the bond is significantly changing. In other words, the barrier region indicates where the bond nature transitions. The barrier is found to be 170 meV above the minimum of the inner well, while the outer well minimum lies at the same height of the inner well minimum, indicating a depth of 170 meV. This implies that the inner and outer wells are in thermal equilibrium and stability is achieved at higher temperature. The excited state has a B2 irreducible representation, which is antisymmetric to inversion across the plane perpendicular to the dimer. This is the representation if the excited electron is in an orbital of σ^* anti-bonding nature for the dimer bond.

To evaluate the optical activity of the surface molecular Si–Si phase, the transition oscillator strength and the corresponding lifetime are calculated. The radiative lifetime τ , the transition matrix

element, and the Einstein coefficient A_{21} for spontaneous decay from the excited state to the ground state are obtained from the oscillator strength f_{osc} . The oscillator strengths obtained allow mapping the radiative rate at each point on the excited state potential energy surface, which determines in which regions emission is most likely to occur. Figure 2(a) also shows the calculated radiative lifetimes of the excited state at varying dimer lengths. The formation of an outer well is encouraging as the radiative rate increases and the lifetime varies by several orders of magnitude along this coordinate path. A sharp increase in the radiative rate is seen near the transition point as well as a smooth increase near the minimum of the outer well. As the barrier is crossed, the lifetime drops from about 25 ns inside the inner well to about 15 ns just after crossing the potential barrier and to about 15 ns at the minimum of the second well. To the left of the barrier, i.e., inside the inner well, where emission has a very long lifetime, is labeled indirect-like (dark state), while to the right of the barrier where emission has a very short lifetime is labeled direct-like (bright state). One can also associate the kink in the ground state curve with the transition in bond nature.

It is to be noted that the electronic and molecular structures of the ground and excited states of the 1-nm silicon nanoparticle with a single H–Si–Si–H structure ($\text{Si}_{29}\text{H}_{34}$) were previously determined using the less accurate Local Density Approximation (LDA) density functional theory and tight binding theory.^{8,9} Qualitatively, the results are similar in terms of two wells connected by a potential barrier. However, quantitatively, there are important differences. The bandgap energy at 2.35 Å obtained with B3LYP is found to be 4.4 eV, which is significantly larger than the 3.5 eV bandgap obtained using LDA.^{8,9} The depth of the outer well is 170 meV significantly shallower than that in the LDA results (700 meV).^{8,9} The potential barrier that connects the two wells is found to be about 0.5 eV relative to the minimum of the inner well. For the 0.5 eV barrier,

quantum tunneling and thermal activation at room temperature are highly weak. However, unlike the present computations, which show that the minima of the two wells are at the same height, it was found that the minimum of the outer well in LDA theory^{8,9} is below that of the inner well by ~ 200 meV, which has implication on the thermal stability of the outer well at higher temperature. These differences affect the time dynamics and spectral distributions. As to the lifetime, LDA calculations are only available for the larger particle of 1.67 nm diameter. In this case, the lifetime was found to be as short as 50 μ s inside the inner well, while it dropped to 1 μ s in the outer well.

One of the difficulties in the single molecular dimer phase model is how to access the outer well through excitation from the ground state of the system. Figure 2(b) shows that the minimum of the outer well in the upper state lies at ~ 3.85 Å, a much larger interatomic separation than that of the ground state ~ 2.35 Å. According to the Frank–Condon principle for molecular species, light absorption is vertical from the minimum of the ground state and the two minima are not lined up; thus, direct excitation into the outer well is not possible. Figure 2(b) labels excitation and emission pathways. It schematically shows two excitation pathways into the inner well: first, minimum-to-minimum vertical excitation followed by quantum tunneling or thermal activation through the barrier; and second, above-barrier excitation at higher photon energy followed by sliding (relaxation) into the outer well. That is, to access the outer well, an indirect path may first take place from the minimum of the ground state to the minimum of the inner well of the excited state. The excitation is expected to be strong. After absorption into the inner well of the excited state, transfer of the population into the outer well must follow. However, the transfer is hindered by the potential barrier (170 meV), which connects the two wells. For 170 meV, quantum tunneling and thermal activation at room temperature are highly weak. This makes emission unlikely. Another feasible path is vertical absorption from the minimum in the ground state well at $R = 2.35$ Å using photon energy at ~ 4.8 to 5 eV (above-barrier excitation) into the repulsive part of the outer well. For illustration, we extended in Fig. 2(b) the outer well in a parabolic fashion to the left (dark dots) to mimic the bond length at which the above-barrier excitation takes place. This excitation is weaker than the minimum-to-minimum excitation, yet it is still sizable. Once excitation takes place, nuclear relaxation (expansion) into the bottom of the outer well follows. The process is expected to give visible emission at 2.76 eV (450 nm) with a Stokes shift of ~ 2 eV. However, experiments given in Sec. V show that, in addition to this excitation, photon energies as low as 3.3–3.5 eV can excite the luminescence with a Stokes shift of ~ 0.6 eV.

B. Coupled dimer networks

The equilibrium ground state geometries for all structures were obtained using DFT with the B3LYP hybrid functional using the quantum chemistry computational package GAMESS (General Atomic and Molecular Electronic Structure System)^{63,64,65} 29 using the 6-311G(d,p) basis set. Given any position for the nuclei, even if not at the minimum of the ground state potential energy surface, time dependent density functional theory (TDDFT) can be used to obtain excited state energies and oscillator strengths. A series of calculations at different nuclear coordinates can therefore

provide the excited state potential energy surface along a slice.

We explore in this section how a 1-nm particle containing multiple H–Si–Si–H molecular dimer sites might affect the energy surfaces, barrier height, and fluorescence dynamics. We employ the same procedure, which we used in Sec. II to create a single dimer-like defect. We use it multiple times to create a network of molecular H–Si–Si–H dimer sites. For example, starting out with $\text{Si}_{29}\text{H}_{36}$ shown in Fig. 3(a), if it is repeated six times, then the number of dimers, namely, six are formed as shown in Fig. 3(b). This is the maximum number of dimers that can be made on the 1-nm particle, and it makes the surface fully reconstructed with only mono-hydride termination remaining. In fact, comparisons of calculated absorption and Raman scattering⁷⁵ have shown that the six-dimer structure is the most likely structure for the 1-nm particles.

We conduct calculations of a 1-nm silicon particle with three different reconstruction dimer configurations as shown in Fig. 4. For comparison, we show in Fig. 4(a) the zero-dimer case $\text{Si}_{29}\text{H}_{36}$. The configurations studied include the (single dimer) one-dimer $\text{Si}_{29}\text{H}_{34}$ structure (presented above in Sec. II) [Fig. 4(b)], five-dimer $\text{Si}_{29}\text{H}_{26}$ structure [Figure 4(c)], and six-dimer $\text{Si}_{29}\text{H}_{24}$ structure [Fig. 4(d)]. The five-dimer case is considered to give information on the trend as dimers are added. For all three cases considered, the coordinates maintained C_{2v} point group symmetry along this path. For those three cases, we employ the improved calculations, which we used in Sec. II.

Figure 5 shows the results for the three cases side-by-side for easy comparison. The partial surface energy diagrams of the Si–Si dimer in the 1-nm particle as a function of the dimer interatomic distance are given, showing the ground state and the lowest excited state along this reaction path. Figure 5(a) shows the results for the single dimer $\text{Si}_{29}\text{H}_{34}$ structure (simplified form of Fig. 2). Possibly due to the increased bandgap according to B3LYP vs LDA, the peak barrier in the single dimer structure is found to be much smaller, only 0.17 eV as opposed to 0.5 eV with LDA. The outer well minimum is found at ~ 3.85 Å, while the depth of the outer well is 0.17 eV.

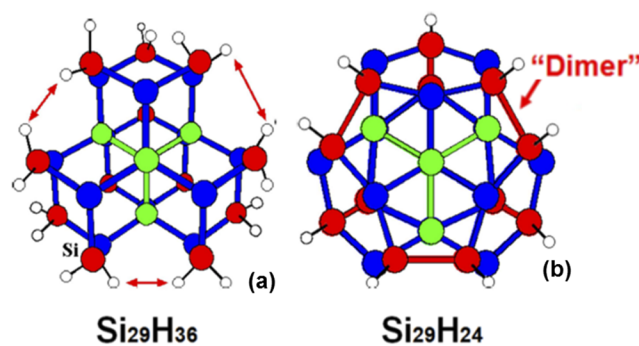


FIG. 3. Configurations of computer models of the H-terminated 1-nm particle. (a) Bulk-like $\text{Si}_{29}\text{H}_{36}$. The double-sided arrows point to three pairs of di-hydride terminated silicon atoms. (b) Fully reconstructed with six dimer bonds (in red) $\text{Si}_{29}\text{H}_{24}$. For each pair of di-hydride terminated silicon atoms in the $\text{Si}_{29}\text{H}_{36}$ "bulk configuration," two hydrogen are removed and the silicon atoms move closer and are bonded (in red). Green, blue, and red are silicon atoms. Smaller white indicate hydrogen atoms. The four green atoms are the central tetrahedral unit. The red atoms are the dimer Si atoms.

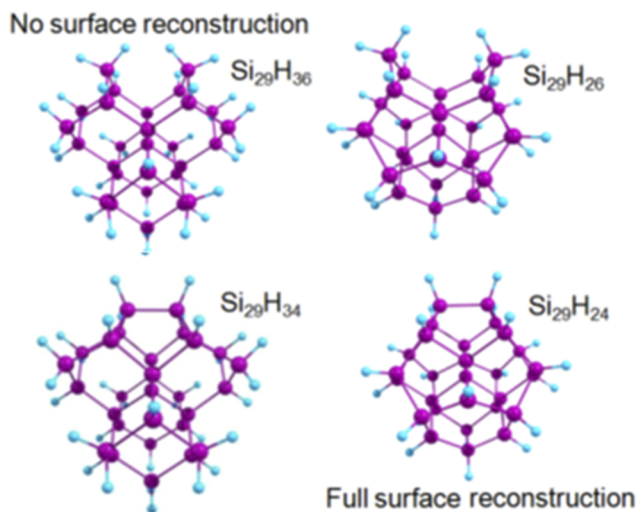


FIG. 4. Computer prototype of the three reconstruction cases Si_{29}H_n in 1-nm particle: $\text{Si}_{29}\text{H}_{34}$ (has one dimer), $\text{Si}_{29}\text{H}_{26}$ (has five dimers), and $\text{Si}_{29}\text{H}_{24}$ (has six dimers). The $\text{Si}_{29}\text{H}_{36}$ is given for reference. Silicon is indicated purple. Hydrogen is indicated in blue.

As mentioned above (Sec. II), the excited state has a B2 irreducible representation, which is antisymmetric to inversion across the plane perpendicular to the dimer. The radiative lifetime for this case is also presented in Fig. 5(a).

As an intermediary case, the five-dimer $\text{Si}_{29}\text{H}_{26}$ structure is studied as shown in Fig. 5(b). The bandgap is found to be 3.5 eV. The potential barrier is only about 85 meV, which is much lower than the single dimer case. As to the double-well structure, the outer minimum appears to be very shallow, with low visibility. The depth of the well has fallen to ~ 10 meV [Fig. 5(b)]. In agreement with the other structures with a surface reconstruction dimer, the radiative lifetime decreases several orders of magnitude as the barrier is approached as shown in Fig. 5(b).

The results for the $\text{Si}_{29}\text{H}_{24}$ structure with a fully reconstructed surface (six dimers, and no remaining di-hydride terminations) are presented in Fig. 5(c). The structure has Td point group symmetry; in addition to simplifying the calculations, this high symmetry makes many of the electronic states degenerate, therefore allowing the calculation of much higher energy states. We calculated the first 28 excited states, with their energies, irreducible representation, and oscillator strengths. There is a band of states from 3.3 to 3.6 eV and then a gap until 4.0 eV. When the structure is broken to C2v symmetry by stretching the dimer, the B2 states arise from Td representations splitting into C2v representations as follows: $\text{T1} \rightarrow \text{A2} + \text{B1} + \text{B2}$ and $\text{T2} \rightarrow \text{A1} + \text{B1} + \text{B2}$. The lowest state is no longer a B2 representation. Only T2 representations are dipole allowed, so the lowest B2 excited state, which originates from T1, is not even dipole allowed. To identify which states participate in the dimer mechanism in this six-dimer structure, the lowest two states of each C2v representation were calculated at several dimer lengths. Again, it is the B2 state that plays a primary role, indicating that the simple picture of σ bonding and σ^* anti-bonding orbitals for a single dimer may still hold even though there are several dimers on the surface. The B2 state crosses the other states to become the lowest excited

state along the majority of this reaction coordinate. This occurs when expanding or contracting the dimer length. When the dimer length is stretched or inflated even longer, the B2 state separates in energy forming a gap from the other states, which remain closely spaced. The outer well now goes lower than the inner well. With the active state verified, more points along the dimer stretch coordinate path are calculated. The resulting slice of the potential energy surface and radiative lifetimes are presented in Fig. 5(c). Because the lowest B2 state is dipole forbidden right at the ground state equilibrium, the first B2 dipole allowed state is used at that point.

As in the single and five dimer cases, there is a drastic decrease in the radiative lifetime as the dimer length approaches and crosses the barrier. To the left of the barrier (in the inner well), the maximum lifetime is about 55 ms, and to the right of the barrier (in the outer well), it reaches a minimum of about 100 ns. The inner well minimum corresponds to the ground state minimum, and the barrier height is now decreased to about 60 meV and it never collapses. While the outer well now goes significantly shallower, (all but disappeared) giving an open state that falls down linearly and below the inner well minimum. In fact, it has disappeared with no longer having a local minimum. At the same time in the same region, the ground state keeps rising linearly, heading for a conic intersection with a linearly rising ground state potential.

The thermal stability in terms of the relative positions of the minima of the inner and outer wells is interesting. The minimum of the outer well is at the same height as that of the inner well (zero difference) for the single dimer case, indicating thermal equilibrium. In the five dimer and six dimer cases, the outer well is very shallow and its minima are below the inner well by 0.4 and 0.3 eV, respectively, indicating thermal stability over the inner well. Attempts to go to longer dimer distances resulted in the hydrogens on the dimer atoms to move to the inside of the dimer, and a smooth transition was not found. Increasing the length further led to the triplet state running into the singlet ground state, making it an unstable reference for TDDFT.¹⁶ This could be interpreted as escape to the outer well, resulting in a non-radiative process of returning to the ground state. We conduct below further studies using relaxation in the excited state to determine if a local minimum in the outer well occurs.

IV. RELAXATION AND OPTIMIZATION IN THE EXCITED STATE (STRUCTURAL TRANSITION BETWEEN INDIRECT AND DIRECT NATURES—STRUCTURAL Q-SWITCHING)

In this section, we choose different computation methods since the previous methods do not allow relaxation in the excited state. Recently, excited state energy gradients with respect to the nuclear positions became available, allowing excited state geometry relaxation. The calculation of the structure optimization of the excited state potential energy surface is done at the TD-DFT level of theory using the B3LYP functional with the TURBOMOLE quantum computational package⁶⁴ and the TZVP basis, which is a triple split valence basis with polarization functions added for each atom.^{65,66,76} Recent studies of small molecules, TDDFT level of theory with the PBE0, CAM-B3LYP, and M06-2X functionals, gave average errors of 1.5%–2%.⁷⁶ To allow a more direct comparison with the previous calculation of the GAMESS 6-311G (d,p), the structure was

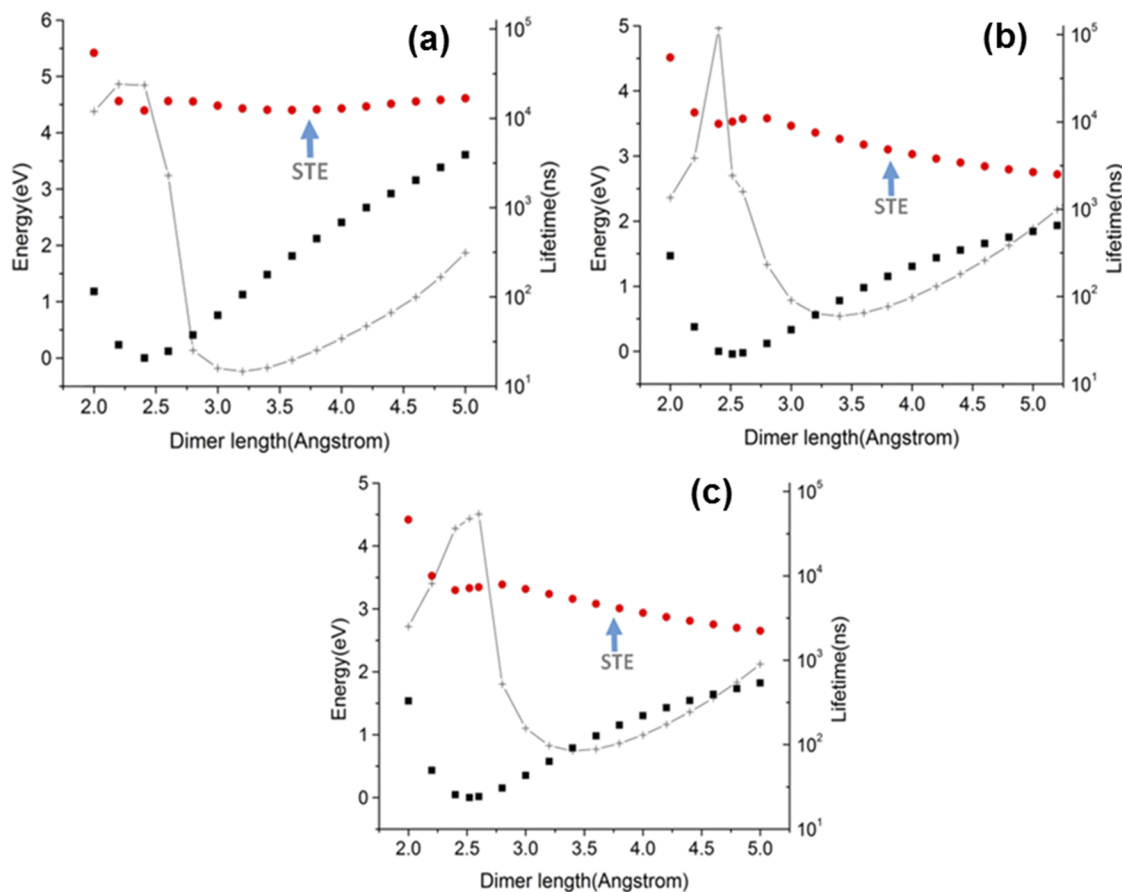


FIG. 5. Potential curves and radiative lifetime of the 1-nm silicon nanoparticle. (■) The ground state and (●) excited state energies relative to the ground state minimum. (+) Lifetime of the lowest excited state as the dimer is stretched. (a) $\text{Si}_{29}\text{H}_{34}$ (has one dimer), (b) $\text{Si}_{29}\text{H}_{26}$ (has five dimers), and (c) $\text{Si}_{29}\text{H}_{24}$ (has six dimers).

constrained to C_{2v} symmetry. We tested the accuracy by calculating the ground state and other levels above the LUMO while optimizing in the ground state of the $\text{Si}_{29}\text{H}_{24}$ using the TURBOMOLE with TZVP basis and the GAMESS 6-311G (d,p). First, the minimum ground state energy structure and the energy of the first excited state T2 were found with this new TURBOMOLE codebase and atomic orbital basis TZVP. The excitation energy with the lowest dipole allowed state (T2 representation) is found to be 3.29 eV above the ground state. In the GAMESS 6-311G (d,p) calculation, the transition was found to be 3.3262. The difference in this bandgap is only 1%. Moreover, the representations of the energy levels are in the same order at least up to the 3.6-eV state, which is the last level below the “gap” to the next band of energy levels. This good agreement indicates the appropriateness of the B3LYP 6-311G (d,p) functional and basis set for the molecular nature of this molecule/solid transition particle.

The path on the excited state surface was now obtained now by minimizing the energy of the first excited state geometry using the TURBOMOLE and the same constraint procedure (with one dimer constrained to a given length). This is carried out to improve on the previously shown $\text{Si}_{29}\text{H}_{24}$ double-well curve [Fig. 5(c)] arrived

at while optimizing in the ground state. This should be a more representative slice of the potential energy surface since the geometries are relaxed in the excited state instead of relaxing in the ground state. To allow a more direct comparison with the previous calculation, the structure was also constrained to C_{2v} symmetry.

Figure 6(a) presents energy level diagrams of the particle, consisting of only the ground and first excited singlet state, with the energies calculated before the particle is excited.⁷⁷ Note that these potential surfaces shown were calculated in both the TURBOMOLE TZVP basis and the GAMESS 6-311G (d,p) basis with a difference of only 1% as was indicated above. The vertical arrow designates the absorption in this system from minimum to minimum. The energy of absorption of this excited state defines the bandgap of the particle. Figure 6(b) presents corresponding energy level diagrams of the particle, with the energies calculated while the particle is excited, consisting of only the ground and first excited singlet state.⁷⁷ Those potential surfaces were calculated by the TURBOMOLE TZVP basis. All energies are relative to the minimum ground state energy in Fig. 6(a), therefore allowing easy comparison and calculation of the emission Stokes shift. The potential surfaces in Fig. 6(b) define the emission. The arrow represent an example of the emission at a

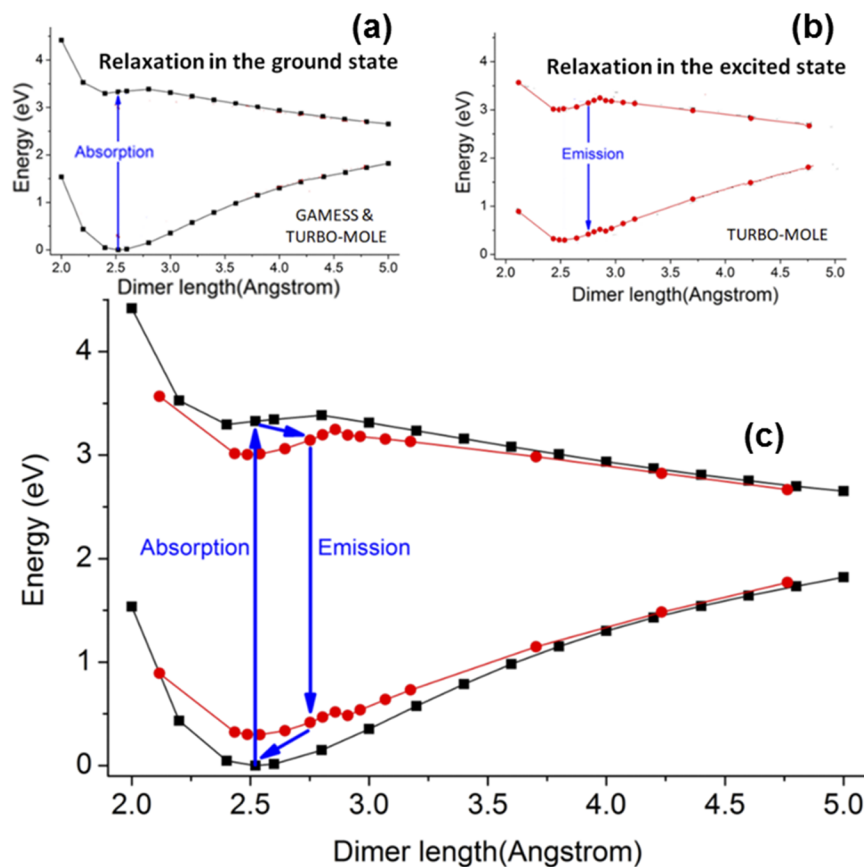


FIG. 6. (a) The ground and excited state energies as a function of the length of a single dimer bond calculated with structures relaxed in the ground state using both the B3LYP functional and the GAMESS and TURBOMOLE packages with 1% difference. (■) Absorption (excitation) proceeds vertically up from the ground state minimum. (b) The ground and excited state energies with structures relaxed in the excited state calculated using the TURBOMOLE package. (●) Emission proceeds vertically down. The structures were calculated with one dimer constrained to a given length and the structure having C_{2v} symmetry. (c) Figures in (a) and (b) are combined. Absorption is a vertical excitation process from the ground state energy minimum to the excited state of that same geometry (optimized in the ground state). The structure (nuclear sites) can then relax/change to one of lower energy in the excited state, where emission occurs vertically to the ground state of this new structure (optimized in the excited state). After emission, the structure (nuclear sites) can then relax back to the ground state minimum. All energies are relative to the ground state minimum optimized in the ground state in (a). In addition, note the four potential surfaces were calculated or verified by the TURBOMOLE package.

particular R in the outer well region. Thus, Figs. 6(a) and 6(b) show that the ground state, which is the highest occupied molecular orbital (HOMO), is calculated twice: before absorption, i.e., before the particle is excited and when the particle is excited. In those two cases, the position of the nuclei is different and transition between the states occurs by simple relaxation of the nuclei. Similarly, the first excited state is calculated twice: before the particle is excited and when the particle is actually excited. The structures were calculated with one dimer stretched and constrained to a given length R and the structure having C_{2v} symmetry. Other features that may be observed in Figs. 6(a) and 6(b) include the following. First, the potential curves for the excited states exhibit a well with a minimum at tetrahedral $R = 2.36$ Å, a barrier at an extended reaction coordinate of $R \sim 3$ Å, and a dissociation limit at ~ 5.4 Å. Second, relaxation in the excited state decreases the inner well of the excited state and increases the energy of the ground state inner well.

Now, we combine the four curves in Fig. 6(c) for easy comparison and analysis and to show several features. Note that the four potential surfaces are essentially calculated using the TURBOMOLE TZVP basis. The figure summarizes the results when optimization of the geometry takes place both in the ground and in the excited state. The potential curves are given as a function of the dimer bond length. Deep in the outer region (beyond the barrier), the energies obtained using optimization in the ground state and excited state converge. Figure 6(c) also shows an example of a pathway

cycle for absorption/relaxation/emission/relaxation. Absorption is a vertical excitation process from the ground state energy minimum (optimized before absorption) to the excited state [of that same geometry (optimized before absorption)]. The structure can then change (relax) causing the excited state (optimized after absorption) to energy-shift to lower energy, where emission occurs to the ground state of this new structure (ground state optimized after absorption) and then will relax back to the initial state (ground state optimized before absorption). Note that the structural relaxation decreased the energy of the excited state in the inner well by an amount equal to 0.28 eV. The relaxation also increased the energy of ground state by 0.30 eV. The total decrease in the emission photon energy is therefore equal to 0.58 eV, which is the Stokes shift of the emission. In the entire inner well and at the barrier, the energy difference between the excited state and ground state remains close to 2.7 eV. Emission at the barrier would be 2.73 eV (455 nm). The emitted photon energy would be therefore overestimated by an energy of 0.58 eV if the particle is not optimized in the excited state.

The instability and structural relaxation may mimic the action or role of the concept of a Q-switch used in laser technology. The dynamic or reversible relaxation allows the stored energy in the long-lived indirect TD well to be released. It is plausible that this phenomenon is behind the stimulated emission, optical gain, or microscopic laser action, which was reported several years back in macroscopic distributions of 1- and 3-nm Si nanoparticles.

The time dynamics of emission is interesting when relaxation in the excited state is accounted for. First, we note that the barrier height between the inner and outer wells for optimization of relaxation in the excited state has now gotten worse, namely increased to 240 meV. This height is measured from the minimum of the inner well of the relaxed excited state as can be seen in Fig. 6(b). This is larger than the depth of 60 meV for optimization of relaxation in the ground state [Fig. 6(a)]. Despite the fact that the inner well becomes deeper against tunneling in the excited state relaxation, direct excitation is energetically allowed because the minimum excitation (absorption) energy of 3.29 eV is higher than the top of the barrier of 3.25 eV of the relaxed excited state as can be easily seen in Fig. 6(c). This means that the system uses nuclei relaxation while in the excited state to avoid the barrier between the indirect and direct natures to allow rapid release of the deposited energy in terms of light. It is to be noted that beyond the barrier in the outer well, the ground state optimized and excited state optimized energies converge, showing that the ground state optimized geometry is a good approximation for the excited state optimized geometry in the outer well. We present in Fig. 7 the calculated energies [given in Fig. 6(b)] and the corresponding radiative lifetimes of the emission as a function of R, along this C2v path with relaxation in the excited state.

The B3LYP-TDDFT calculations presented above show that the barrier height has been reduced to 60 meV for the maximum number of dimer sites that can be constructed, making it more accessible than the 0.5 eV barrier calculated using LDA for a single dimer.^{8,9} However, it is still high enough to allow transfer of the population from the inner well to the outer well, i.e., complete transition from indirect to direct nature. Thus, the excitation stays the same as the rate of emission in the inner well is very slow because of the indirect nature and because the tunneling through the barrier or thermal activation over it are also slow. Moreover, although an exciton can

migrate, large distances in bulk and most likely can encounter an impurity site, even for a low impurity density, allowing its energy to be dissipated; it is highly unlikely to find an extrinsic impurity in an ultrasmall nanoparticle due to spatial confinement, and as such ruling out this dissipation channel. Under these conditions, the particle cannot release the energy according to a single dimer model. Due to this instability, another mechanism takes place, which may allow the system to bypass or overcome the potential barrier, allowing population transfer from the inner to the outer well at room temperature, hence releasing the trapped energy. The mechanism is further relaxed while the particle is in the excited state.

V. EFFECT OF STRUCTURAL SYMMETRY

In the above computations of Si₂₉H₂₄ with six dimers, we adopted the specific symmetry of C_{2v} during excitation and emission. Without symmetry constraints, relaxing the particle while in the lowest excited state resulted in a geometry with Cs symmetry. The results are shown in Fig. 8, which presents the ground and first excited state as a function of R for this symmetry. The barrier height is 120–130 meV. A small kink in the ground state energy is seen at about 3.0 Å along these excited state optimized paths. This is due to the “direction” in nuclear coordinate space not being just a straight line. Near the barrier peak, the ground state energy briefly decreases even though the dimer is being stretched further. This indicates that the outer well is closer to the ground state minimized structure (at that dimer length) than the inner well structure is. This seems to be a generic feature as this kink is seen in all the excited state optimized paths.

Figure 8 also presents the calculated emission lifetime as a function of R along the Cs double-well path. It is to be noted that the lifetime drops several orders of magnitude as the dimer length increases past the barrier length. The lifetime minimum is on the order of 100 ns. Emission at the barrier would be 2.52 eV (490 nm), while

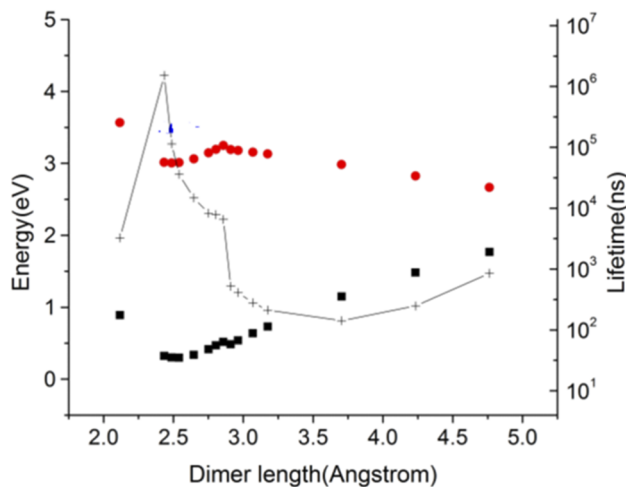


FIG. 7. Emission lifetime for 1 nm Si₂₉H₂₄ relaxed in the excited state. Geometries obtained by relaxing the particle in the first excited state with one dimer constrained to a given length and the structure having C_{2v} symmetry [as in Fig. 6(b)]. Radiative lifetime (+). The ground state (■) and first two excited states (●) energies relative to the ground state minimum, optimized in the ground state shown in Fig. 6(a).

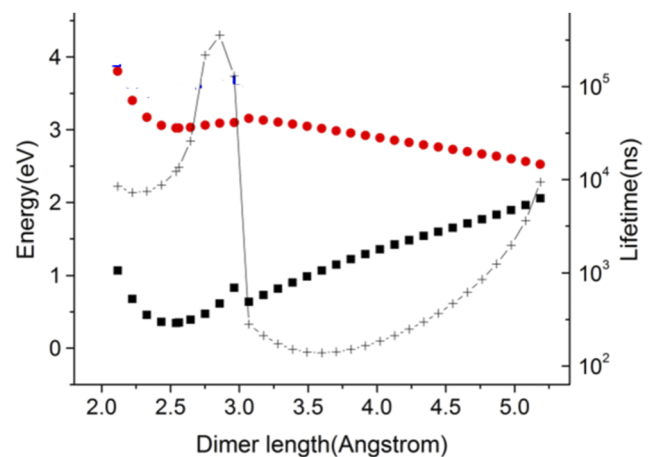


FIG. 8. Emission lifetime for 1 nm Si₂₉H₂₄ relaxed in the excited state. Geometries obtained by relaxing the particle in the first excited state with one dimer constrained to a given length and the structure having Cs symmetry. Radiative lifetime (+). The ground state (■) and first two excited states (●) energies relative to the ground state minimum, optimized in the ground state of C_{2v} symmetry shown in Fig. 6(a).

emission from the structure on the path with the shortest lifetime would be 1.95 eV (640 nm). The outer well was found to be very shallow (half-open), i.e., to have no minimum. Along the double-well path, at about 5.2 Å the structure becomes unstable to relaxing with the excited state (A_2 representation) running into the singlet ground state (A_1 representation).

Generally, the Cs symmetry gave slightly lower energies for excitation and emission, indicating that the C_{2v} symmetry is not the minimum energy structures. The lower ground state energy of this path reduces the Stokes shift. In fact, after a close comparison of the Cs and C_{2v} energy surfaces, we observe that at the inner well minimum, the ground state energy of the Cs double-well path is 50 meV lower than that of the C_{2v} path. However, the excited state energies are nearly degenerate, with some portions of the Cs inner well lower in energy than the corresponding dimer length structure of C_{2v} symmetry while other portions are slightly higher in energy. Therefore, if the structure relaxes into the “trough” of the Cs double-well path, the C_{2v} double-well path is energetically accessible as well. If there are many local minima in the excited state surface near the barrier peak, the large change in the ground state energy (~ 0.25 eV) between the two known Cs troughs indicates that such a scenario could help explain the large range of Stokes shift. The Cs double-well barrier has an emission of 455 nm, and the C_{2v} double-well barrier has an emission of 490 nm.

VI. EXPERIMENTAL MEASUREMENTS

We used electrochemical etching in an $\text{HF}/\text{H}_2\text{O}_2$ mixture to disperse crystalline Si into nanoparticles (5–7). The wafer was laterally anodized while being advanced slowly into the solution. Because HF is highly reactive with silicon oxide, H_2O_2 increases the etching rate, thus producing smaller particles. Moreover, the oxidative nature of the peroxide removes di-hydride and tri-hydride terminations and hence produces chemically and electronically high quality particles. The particles are H-passivated with a mono-hydride. The treated Si wafer was then transferred to an ultrasound bath under which the particles dislodged into a colloidal suspension in isopropyl alcohol. High-resolution TEM was used to image the particles as shown in Fig. 1(a). A most probable prototype of the 1-nm nanoparticle was determined using quantum Monte Carlo simulations to be $\text{Si}_{29}\text{H}_{24}$ configuration¹¹ as depicted in Fig. 1(b).

The photoluminescence spectra of a colloid in isopropyl alcohol were recorded under ambient conditions using a photon counting spectrofluorometer with a Xe arc-lamp light source excitation and 4 nm bandpass excitation and emission monochromators. The emission spectrum from one of the samples under 350 nm UV excitation is shown in Fig. 9(a). A distinct emission band is observed centered at 440 nm and a weaker band at 480 nm.

The response of the silicon nanoparticles in the range of 120–255 nm cannot be measured under ambient or wet conditions

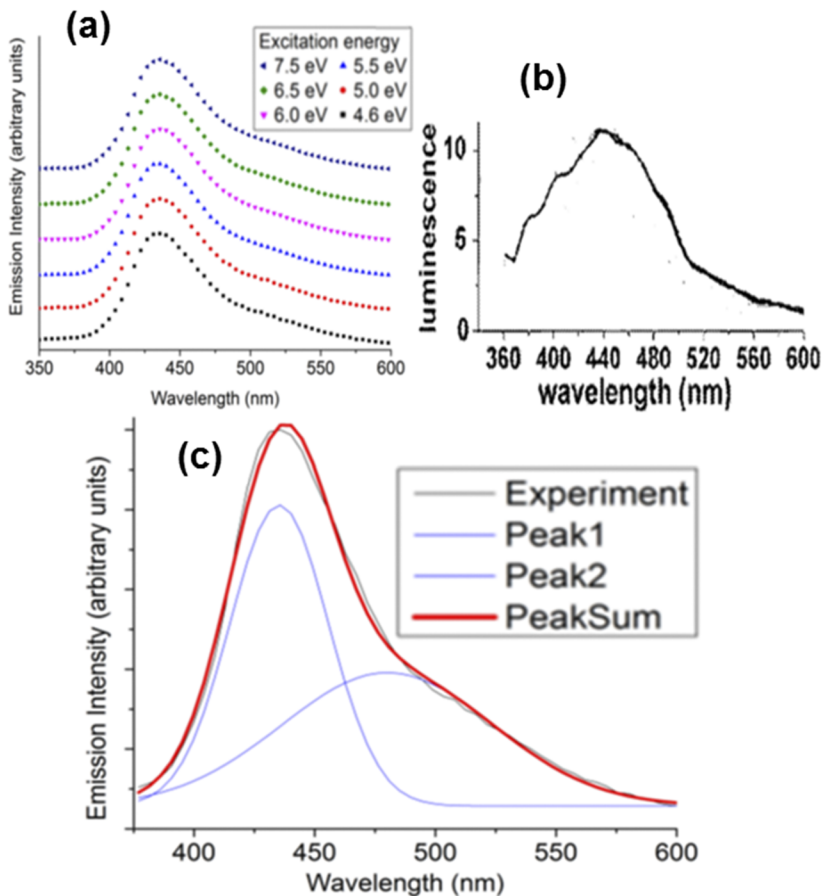


FIG. 9. The photoluminescence spectra of the 1-nm silicon nanoparticle for several excitation photon energies. (a) Under (3.5 eV) 350 nm UV excitation of a wet sample at room temperature and (b) under excitation energy in the range of 4.6–7.5 eV of a thin films under vacuum at 10 K. Spectra have been vertically offset for ease of comparison. (c) Gaussian fitting of the photoluminescence spectrum under 4.6-eV excitation using two Gaussians giving fitted peaks at 435 and 480 nm.

because of light propagation problems. In this range, we measured the response at the Daresbury Synchrotron Radiation Source facility in the UK. The sample chamber has non-bake base pressures of typically 10^{-8} Torr at room temperature (300 K°) or $<10^{-10}$ Torr at 10 K° . The setup included a five-m normal incidence concave grating monochromator. Two interchangeable gratings cover the photon energy range of 5–35 eV (or, equivalently, 2500–350 Å) with a best achievable resolution of 2 meV (0.05 A°). A peak flux of 1.4×10^{12} photons/s, for a stimulated Synchrotron Radiation Source (SRS) stored beam current of 200 mA, has been measured at around 23 eV. For detection over extended photon ranges, GaAs-based photocathode tubes are used (GaAs and GaInAs:Ce). At room temperature, the GaAs tube, with a typical gain of 10^7 , has dark counts of around 300 counts s^{-1} . It has a gain of 1.6×10^5 , with dark counts of 50 when cooled to 258 K° . The chamber incorporates a compact low-temperature UHV-compatible cryostat. A two-stage closed-cycle refrigerator allows regulation of the temperature of sample in the range of 7–330 K° . Typical cool-down times to 10 K° are 90 min.

Thin films were formed on silicon wafers using simple drop evaporation starting from the suspension. After the particles were dried well on a substrate, they were placed in the vacuum chamber and cooled to 10 K° . The emission in response to a range of excitation energies is shown in Fig. 9(b). The emission spectra are found to be largely independent of excitation energy in the range from 4.6 to 7.5 eV. This is due to the fact that in such a range, above-barrier excitation takes place followed by relation to the top of the barrier region. The emission appears to be a band near 435–440 nm with a shoulder in the longer emission wavelengths. The emission fits well with two Gaussians as shown in Fig. 9(c). The fitted peaks are at 435 and 480 nm, with full width-half maximum values of 48 and 103 nm, respectively. The fit error for the center location of the peaks is less than 1 nm for the main 435 nm peak and 6 nm for the broad 480 nm peak. This fits the prediction of two peaks although the predicted wavelengths were overestimated by 20 and 10 nm, respectively.

VII. DISCUSSION

We present in Table I the calculated bandgap, the barrier height, the depth of the outer well, the Stokes shift, and emission lifetime against the number of molecular sites for 1-nm nanoparticles. The table shows that the bandgap and Stokes shift drop with the number of dimer sites, trends that are in the right direction from the point of view of experiment. It is to be noted that the maximum number of dimer-like sites that can be reconstructed in the 1-nm

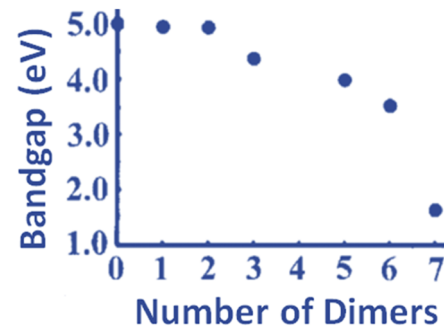


FIG. 10. Calculated bandgap of 1-nm silicon nanoparticle as a function of the number of the reconstruction surface dimers.

particle is six (removal of 12 hydrogen atoms starting out from 36, with 24 H atoms remaining) and that the bandgap drops slowly from 4.4 for a single dimer to 3.3 for six dimers. Upon removal of more than 12 H atoms (less than 24 remaining H atoms or >six new Si–Si bonds formed), the bandgap drops sharply, approaching zero, the metallic zero bandgap as shown in Fig. 10.^{11,29} The sharp drop is due to the fact that bonding of those resulting dangling bonds is carbon-like sp^2 .

As to the barrier height, the table shows that it drops from 170 to 60 meV with the increasing number of dimer sites from 1 to 6. However, the barrier remains sizable. This limits the transfer of population from the absorption well to the emission well. In fact, for efficient tunneling or thermal activation to proceed significantly at room temperature, the barrier must be well below $kT \sim 30$ meV. However, the finite limit is necessary if the molecular direct nature is to survive.

With regard to the depth of the emission (outer/molecular) well, Table I and Fig. 5 show that the outer well becomes shallower and shallower as the number of dimer sites increases. In fact, the depth for the six-dimer case ($Si_{29}H_{24}$ structure) nearly disappears, opening the well on one side and allowing it to fall linearly, where it crosses at large R the linearly rising ground state in a conical fashion. Having no minimum may imply that the outer well cannot trap the photo-excited excitons (unstable well), i.e., the self-trapped exciton model may fail. Moreover, the conical intersection of the excited state with the ground state implies that relaxation after crossing the barrier leads to non-radiative recombination back to the ground state potential energy surface. Since internal conversion

TABLE I. Calculated bandgap, the barrier height, the depth of the outer well, the Stokes shift, and emission lifetime against the number of molecular sites for 1-nm nanoparticles.

Molecular dimer number	1-nm Si nanoparticle				
	Bandgap (eV)	Stokes shift (eV)	Barrier height (meV)	Emission lifetime (ns)	Molecular well depth (meV)
One-dimer $Si_{29}H_{34}$	4.4	1.5–2.0	170	15	170
Two-dimer $Si_{29}H_{26}$	3.5	0.6	85	75	30
Three-dimer $Si_{29}H_{24}$	3.4	0.5	60	90	10

happens on the order of picoseconds,⁷⁸ orders of magnitude faster than the radiative lifetime, it guarantees that relaxation in the outer well would not result in emission. Another feature worth mentioning is that correlating with the shallowing of the outer well, the emission slows down, increasing the emission lifetime. However, despite the disappearance of the minimum (loss of stability of the well), the lifetime increases from 15 ns for one dimer to only 90 ns for six dimers. This observation points to the conclusion that the system does not expand to the dissociation or the conical intersection region fully. Moreover, the limited increase in the emission lifetime may indicate that a minimum in the molecular bonds is not necessary for radiative recombination of excitons to proceed. It is plausible that “self-trapping” can still take place and emission may be commencing near the transition (barrier) region, and as such the molecular model remains valid.

The finite and non-vanishing potential barrier is an indication that the molecular direct nature survives and that trapping may still occur. We now present the charge distribution in the $\text{Si}_{29}\text{H}_{24}$ particle, obtained from the calculated wavefunctions, to evaluate the implication of the openness of the emission well to the ability to trap the excited electron-hole pair (exciton). Figure 11(a) shows the charge distribution for a dimer bond (reaction coordinate) of 2.4 Å (un-stretched dimer, at the bottom of the inner well).¹⁶ The HOMO [singlet hole ground state (valence band)], given on the left of Fig. 11(a), and the LUMO [singlet electron excited state (conduction band)], given on the right of Fig. 11(a), show that the

electron and the hole are delocalized throughout the nanoparticle. For a stretched dimer at separations ~ 3 Å (near the top of the barrier transition region) as shown in Fig. 11(b), the hole and electron become concentrated (trapped) on the stretched dimer. Thus, despite the fact that the outer well has no minimum (very shallow), trapping takes place in the transition barrier region. When confined on the same dimer, i.e., electron and hole, being in the same place at the same time, the respective wave functions overlap, increasing the exchange integral, and hence the radiative recombination rate.

Figure 6 provides an alternative mechanism to thermal activation or quantum tunneling for accessing the top of the barrier. Unlike bulk where excitons can non-radiatively release absorbed energy through two electron processes and at doping impurities through migration over large distances, the absorbed energy in nanostructures remains held up due to diminishment of the rate of non-radiative processes and lack of impurities due to spatial confinement, creating a structural instability. The multiplicity alleviates the structural strain and instability by allowing the excited particle to structurally relax to shift the state to lower energy with a variety of symmetries. This causes the absorbed energy to be transferred into the top of the transition barrier region of the shifted lower state, followed by strong and fast emission without the need for crossing any barrier. For instance, Fig. 6 shows that upon excitation, the deposited photon energy is trapped (stored) in the bottom of the inner well, which causes a sizable strain and structural instability. The present computations show that the structural instability in the excited state

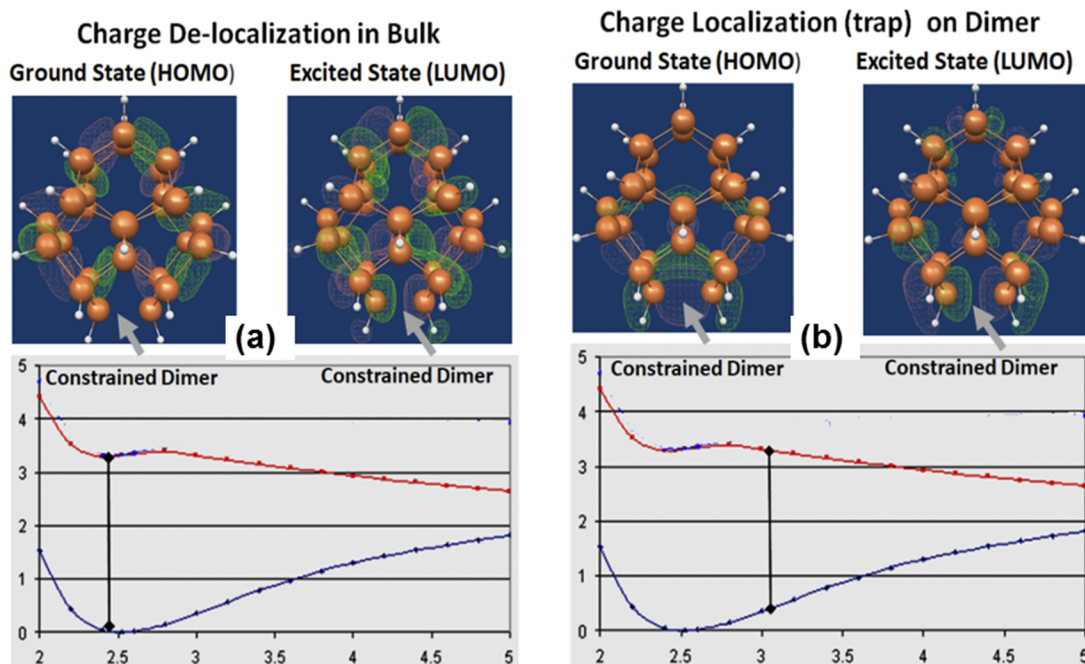
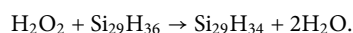


FIG. 11. Electron and hole charge distribution in the 1-nm Si nanoparticle before and after excitation. (a) Before excitation at 2.4 Å un-stretched dimer, at the bottom of the inner well for the electron in the LUMO conduction band (**top**) and for the hole in the HOMO valence band (**bottom**). (b) Just after excitation at 3 Å stretched dimer, just beyond the top of the potential barrier for the electron in the LUMO conduction band (**top**) and for the hole in the HOMO valence band (**bottom**). It displays the de-localization throughout the particle before excitation and trapping or localization on the dimer after excitation. Charge distribution (Green), silicon atoms (orange), and hydrogen atoms (white).

causes the excited particle to relax structurally to a lower lying potential surface (state), releasing the trapped energy from the bottom of the well to the transition region near the top of the barrier of the lower lying relaxed excited state. Consequently, the process allows fluorescence to commence without the need for thermal activation or crossing the barrier via tunneling. Moreover, the results point to the fact that there is enough mixing of the emission and absorption wave functions in the transition region allowing for strong recombination/emission with nanosecond dynamics to proceed. Fast emission in the transition region avoids the non-radiative recombination (quenching of emission) at the conical intersection, perhaps avoiding dissociation of the bond into dangling electron bonds that may be susceptible to environmental attacks.

These studies therefore point to the plausibility of the direct-like molecular phase to account for the measured optical characteristics of the ultrasmall silicon nanoparticles including direct-like emission, broadband visible spectrum, nanosecond time dynamics, ultraviolet (UV) radiation covering the A wavelength range 315–400 nm (UVA) excitation edge, half eV Stokes shift.

Previous computation results shed light on the keys to synthesis of the nanoparticles. Those showed that the interaction of H₂O₂ with Si₂₉H₃₆ strips two hydrogen atoms to form two free-standing water molecules, while the “stripped” nearby Si atoms move appreciably closer to each other (allowed by significant loss of elasticity in sub-3-nm particles) to form Si₂₉H₃₄ particles having a dimer-like molecular bond H–Si–Si–H,



This reaction proceeds in a spontaneous manner under the experimental synthesis protocol and is supported by the thermodynamics computations of the reconstruction.¹⁵ First, within GGA computation methods, the total energies of the “reaction” Si₂₉H₃₆ → Si₂₉H₃₄ + H₂ have a balance of ~–0.3 eV (endothermic at T = 0) and therefore such a dimerization may well occur for suitable chemical potentials of hydrogen. Second, since the oxygen–oxygen distance in H₂O₂ fits reasonably well with the neighboring hydrogens on the two Si atoms, such a reaction suggests a short reaction path. Third, the process is exothermic in GGA by ~2.7 eV.⁷⁹

VIII. CONCLUSION

We studied 1-nm hydrogenated Si particles with a surface network of coupled H–Si–Si–H created by reconstruction, both theoretically and experimentally. We used laboratory and synchrotron UV excitation as well as first-principles atomistic simulations and computations. We used in the TDDFT computations the B3LYP hybrid functional and both the quantum computational package GAMESS (General Atomic and Molecular Electronic Structure System) using the 6-311G(d,p) basis set and the TURBOMOLE quantum computational package with the TZVP basis set. The results show that due to a structural instability in the excited state, the optimization processes give two distinct nuclear structures in the potential surfaces against the inflation of the dimer bond of the ground and excited states. However, both show potential barriers between the excitation and emission channels. The structural relaxation in the excited state creates a direct path for releasing excitations by radiative emission, which otherwise would be trapped by the potential barrier. Following emission, the particle relaxes back

to the indirect ground structure, which completes the cycle. The results also confirm the pivotal role of HF/H₂O₂ etching in synthesizing the core–shells and affording control over the molecular network. Measurements using synchrotron and laboratory UV excitation of thin films of 1-nm Si particles show good agreement with the simulation results. The distinct nuclear geometries of the excited and ground states and relaxations between them can account for the stimulated emission, gain, or microscopic laser action, reported earlier in macroscopic distributions of 1- and 3-nm Si nanoparticles.

DATA AVAILABILITY

The data that support the findings of this study are available from the corresponding author upon reasonable request.

REFERENCES

- O. Ackakir, J. Therrien, G. Belomoin, N. Barry, J. Muller, E. Gratton, and M. Nayfeh, *Appl. Phys. Lett.* **76**, 1857–1859 (2000).
- A. Smith, S. Rao, S. Chaieb, and M. H. Nayfeh, *Appl. Phys. Lett.* **80**, 841 (2002).
- D. Nielsen, L. Abuhassan, M. Alchihabi, A. Al-Muhanna, J. Host, and M. H. Nayfeh, *J. Appl. Phys.* **101**(11), 114302 (2007).
- L. T. Canham, *Appl. Phys. Lett.* **57**(10), 1046–1048 (1990).
- Functionalization, and Surface Treatment of Nanoparticles*, edited by M. I. Baratron (American Scientific Publishers, 2002).
- M. H. Nayfeh, L. Mitas, and V. Kumar, *Silicon Nanoparticles: New Photonic and Electronic Material at the Transition between Solid and Molecule* (Elsevier, 2007).
- M. H. Nayfeh, *Fundamentals and Applications of Nano Silicon in Plasmonics and Fullerenes: Current and Future Trends* (Elsevier Publishing, 2018).
- G. Allan, C. Delerue, and M. Lannoo, *Phys. Rev. Lett.* **76**, 2961 (1996).
- M. Lannoo, C. Delerue, and G. Allan, “Theory of radiative and nonradiative transitions in for semiconductor nanocrystals,” *J. Lumin.* **70**, 170 (1996).
- M. H. Nayfeh, N. Rigakis, and Z. Yamani, *Phys. Rev. B* **56**, 2079 (1997).
- L. Mitas, J. Therrien, R. Twisten, G. Belomoin, and M. H. Nayfeh, *Appl. Phys. Lett.* **78**, 1918 (2001).
- E. W. Draeger, J. C. Grossman, A. J. Williamson, and G. Galli, *Phys. Rev. Lett.* **90**, 167402 (2003).
- D. Sundholm, *Nano Lett.* **3**, 847 (2003).
- S. Rao, J. Sutin, R. Clegg, E. Gratton, M. H. Nayfeh, S. Habbal, A. Tsolakidis, and R. M. Martin, *Phys. Rev. B* **69**, 205319 (2004).
- L. Wagner, A. Puzder, A. Williamson, S. Helms, J. C. Grossman, L. Mitas, G. Galli, and M. Nayfeh, *arXiv:cond-mat/0403226v1* [cond-mat.mtrl-sci] (2004).
- J. Malloy, K. Mantey, Y. Maximenko, E. Bahceci, H. Morgan, Z. Yamani, J. Boparai, K. Puthalath, and M. H. Nayfeh, *J. Appl. Phys.* **124**, 044501 (2018).
- O. M. Nayfeh, S. Rao, A. Smith, J. Therrien, and M. H. Nayfeh, *IEEE Photonics Technol. Lett.* **16**, 1927 (2004).
- S. Magill, J. Xie, M. Nayfeh, H. Yu, M. Fizari, J. Malloy, and Y. Maximenko, *J. Instrum.* **10**, P05008 (2015); M. H. Nayfeh, S. Rao, O. M. Nayfeh, A. Smith, and J. Therrien, *IEEE Trans. Nanotechnol.* **4**, 660 (2005).
- M. H. Nayfeh, N. Barry, J. Therrien, O. Akcakir, E. Gratton, and G. Belomoin, *Appl. Phys. Lett.* **78**, 1131 (2001).
- M. H. Nayfeh, O. Akcakir, G. Belomoin, N. Barry, J. Therrien, and E. Gratton, *Appl. Phys. Lett.* **77**, 4086 (2000).
- M. Stupca, O. M. Nayfeh, T. Hoang, M. H. Nayfeh, B. Alhreish, J. Boparai, A. Aldwayyan, and M. AlSalhi, *J. Appl. Phys.* **112**, 074313 (2012).
- O. M. Nayfeh, D. A. Antoniadis, K. Mantey, and M. H. Nayfeh, *Appl. Phys. Lett.* **90**, 153105 (2007).
- Q. Liu, M. H. Nayfeh, and S.-T. Yau, *J. Power Sources* **195**, 3956–3959 (2010).
- M. Stupca, M. Alsalhi, T. Al Saud, A. Almuhanna, and M. H. Nayfeh, *Appl. Phys. Lett.* **91**, 063107 (2007).
- G. Wang, K. Mantey, M. H. Nayfeh, and S.-T. Yau, *Appl. Phys. Lett.* **89**, 243901 (2006).

- ²⁶Y. Choi, G. Wang, M. H. Nayfeh, and S.-T. Yau, *Biosens. Bioelectron.* **24**, 3103 (2009).
- ²⁷K. Mantey, A. Zhu, B. Jack, M. Nayfeh, C. Marsh, and G. Al Chaar, *Phys. Rev. B* **85**, 085417 (2012).
- ²⁸A. Smith, Z. H. Yamani, N. Roberts, J. Turner, S. R. Habbal, S. Granick, and M. H. Nayfeh, *Phys. Rev. B* **72**, 205307 (2005).
- ²⁹S. G. Balasubramani *et al.*, *J. Chem. Phys.* **152**, 184107 (2020).
- ³⁰G. Belomoin, E. Rogozhina, J. Therrien, P. V. Braun, L. Abuhassan, M. H. Nayfeh, L. Wagner, and L. Mitás, *Phys. Rev. B* **65**, 193406 (2002).
- ³¹J. P. Proot, C. Delerue, and G. Allan, *Appl. Phys. Lett.* **61**(16), 1948 (1992).
- ³²L. W. Wang and A. Zunger, *J. Phys. Chem.* **98**(8), 2158 (1994).
- ³³M. Rohlfling and S. G. Louie, *Phys. Rev. Lett.* **81**(11), 2312 (1998).
- ³⁴L. X. Benedict, A. Puzder, A. J. Williamson, J. C. Grossman, G. Galli, J. E. Klepeis, J. Y. Raty, and O. Pankratov, *Phys. Rev. B* **68**(8), 085310 (2003).
- ³⁵B. Delley and E. F. Steigmeier, *Phys. Rev. B* **47**(3), 1397 (1993).
- ³⁶S. Ogut, J. R. Chelikowsky, and S. G. Louie, *Phys. Rev. Lett.* **79**(9), 1770 (1997).
- ³⁷I. Vasiliev, *Phys. Status Solidi B* **239**(1), 19 (2003).
- ³⁸A. J. Williamson, J. C. Grossman, R. Q. Hood, A. Puzder, and G. Galli, *Phys. Rev. Lett.* **89**(19), 196803 (2002).
- ³⁹G. Al-Chaar, T. Hoang, D. Dowds, K. Ford, T. Carlson, and C. Marsh, *J. Cluster Sci.* **25**, 559 (2014).
- ⁴⁰D. A. Smith, University of Illinois at Urbana-Champaign. ProQuest Dissertations Publishing, 3314897, (2008).
- ⁴¹J. Therrien, "Size dependence of the electrical characteristics of silicon nanoparticles," Ph.D. thesis, University of Illinois at Urbana-Champaign, Champaign, IL, 2003.
- ⁴²C. Delerue, G. Allan, and M. Lannoo, *Phys. Rev. B* **48**, 11024 (1993).
- ⁴³A. Puzder, A. Williamson, J. Grossman, and G. Galli, *J. Am. Chem. Soc.* **125**, 2786 (2003).
- ⁴⁴A. Puzder, A. Williamson, F. Reboredo, and G. Galli, *Phys. Rev. Lett.* **91**, 157405 (2003).
- ⁴⁵E. Draeger, J. Grossman, A. Williamson, and G. Galli, *J. Chem. Phys.* **120**, 10807 (2004).
- ⁴⁶I. Vasiliev and R. M. Martin, *Phys. Status Solidi B* **233**(1), 5 (2002).
- ⁴⁷M. Nishida, *Phys. Lett. A* **323**, 449 (2004).
- ⁴⁸M. Nishida, *Phys. Rev. B* **69**(16), 165324 (2004).
- ⁴⁹M. Nishida, *J. Appl. Phys.* **99**, 053708 (2006).
- ⁵⁰C. S. Garoufalis and A. D. Zdetsis, *Phys. Chem. Chem. Phys.* **8**, 808 (2006).
- ⁵¹I. Vasiliev, J. R. Chelikowsky, and R. M. Martin, *Phys. Rev. B* **65**(12), 121302 (2002).
- ⁵²C. S. Garoufalis and A. D. Zdetsis, *J. Math. Chem.* **46**(3), 952 (2009).
- ⁵³A. Tsolakidis and R. M. Martin, *Phys. Rev. B* **71**(12), 125319 (2005).
- ⁵⁴O. Lehtonen and D. Sundholm, *Phys. Rev. B* **72**(8), 085424 (2005).
- ⁵⁵N. U. Zhanpeisov and H. Fukurnura, *J. Nanosci. Nanotechnol.* **8**(7), 3478 (2008).
- ⁵⁶S. Rao, "A study of the molecular behavior in the vibronic and excitonic properties of silicon nanoparticles," Ph.D. thesis, University of Illinois at Urbana-Champaign, Champaign, IL, 2006.
- ⁵⁷T. M. Duarte, P. G. C. Buzolin, I. M. G. Santos, E. Longo, and J. R. Sambrano, *Theor. Chem. Acc.* **135**, 151 (2016).
- ⁵⁸J. Maul, I. M. G. Santos, J. R. Sambrano, and A. Erba, *Theor. Chem. Acc.* **135**, 36 (2016).
- ⁵⁹J. Maul, A. Erba, I. M. G. Santos *et al.*, *J. Chem. Phys.* **142**, 014505 (2015).
- ⁶⁰E. Heifets, R. I. Eglitis, E. A. Kotomin *et al.*, *Sur. Sci.* **513**, 211 (2002).
- ⁶¹E. Heifets, W. A. Goddard, E. A. Kotomin *et al.*, *Phys. Rev. B* **69**, 235417 (2004).
- ⁶²J. Paier, *J. Chem. Phys.* **127**, 024103 (2007).
- ⁶³S. Tomi and N. M. Harrisona, <https://citeseerx.ist.psu.edu>.
- ⁶⁴TURBOMOLE V6.3 2011, a development of University of Karlsruhe and Forschungszentrum Karlsruhe GmbH, 1989–2007, TURBOMOLE GmbH, since 2007; available from <http://www.turbomole.com>.
- ⁶⁵F. Weigend and R. Ahlrichs, *Phys. Chem. Chem. Phys.* **7**, 3297 (2005).
- ⁶⁶F. Weigend, M. Haser, H. Patzelt, and R. Ahlrichs, *Chem. Phys. Lett.* **294**, 143 (1998).
- ⁶⁷A. Schafer, C. Huber, and R. Ahlrichs, *J. Chem. Phys.* **100**, 5829 (1994).
- ⁶⁸L. Zhao and E. Neuscammann, *J. Chem. Theory Comput.* **16**(1), 164 (2020).
- ⁶⁹G. Levi, *Faraday Discuss.* **224**, 448 (2020).
- ⁷⁰E. R. Davidson and D. Feller, *Chem. Rev.* **86**(4), 681 (1986).
- ⁷¹Atomic Simulation Environment, <https://wiki.fysik.dtu.dk/ase/ase/dft/bztable.html>, Last updated on Sun, 18 Jul 2021.
- ⁷²M. W. Schmidt, K. K. Baldrige, J. A. Boatz, S. T. Elbert, M. S. Gordon, J. H. Jensen, S. Koseki, N. Matsunaga, K. A. Nguyen, S. J. Su, T. L. Windus, M. Dupuis, and J. A. Montgomery, *J. Comput. Chem.* **14**, 1347 (1993).
- ⁷³M. S. Gordon and M. W. Schmidt, *Advances in Electronic Structure Theory: GAMESS a Decade Later* (Elsevier, Amsterdam, 2005).
- ⁷⁴See <http://www.msg.ameslab.gov/games/gamess.html> for Ab initio quantum code GAMESS (General Atomic and Molecular Electronic Structure System) to the PowerMac of Mark Gordon's research group at Iowa State University.
- ⁷⁵S. Rao, K. Mantey, J. Therrien, A. Smith, and M. Nayfeh, *Phys. Rev. B* **76**, 155316 (2007).
- ⁷⁶A. Schäfer, H. W. Horn, and R. Ahlrichs, *J. Chem. Phys.* **97**, 2571 (1992);
- ⁷⁷K. A. Mantey, "Structure, electronic levels, and ionic interactions of Inanometer silicon particles," Ph.D. dissertation (University of Illinois at Urbana-Champaign, 2011).
- ⁷⁸J. R. Lakowicz, *Principles of Fluorescence Spectroscopy*, 3rd ed. (Springer, New York, NY, 2006).
- ⁷⁹A. Puzder, A. J. Williamson, J. C. Grossman, and G. Galli, *J. Chem. Phys.* **117**, 6721 (2002).